



Supplement of

Real-world observations of reduced nitrogen and ultrafine particles in commercial cooking organic aerosol emissions

Sunhye Kim et al.

Correspondence to: Albert A. Presto (apresto@andrew.cmu.edu)

The copyright of individual parts of the supplement might differ from the article licence.

1. Sampling details



Figure S1. Example of mobile laboratory sampling from a restaurant exhaust plume. This photo shows the mobile laboratory parked near the restaurant location identified as “Pizza” in Table 1 and is collecting data on the plume source. The sampling inlet is located on top of the mobile laboratory. This restaurant emitted a visible plume of cooking emissions; the visible extent of the plume is shown by the white dashed line. The cooking emissions had a major impact on local PM concentrations in the alleyway where we conducted our sampling. PM_{2.5} mass concentrations in the alley routinely exceeded 100 $\mu\text{g m}^{-3}$ at a location approximately 10 m from the restaurant (Tanzer et al., 2019) exhaust.

References:

Tanzer, R., Malings, C., Hauryliuk, A., Subramanian, R., & Presto, A. A. (2019). Demonstration of a Low-Cost Multi-Pollutant Network to Quantify Intra-Urban Spatial Variations in Air Pollutant Source Impacts and to Evaluate Environmental Justice. *International Journal of Environmental Research and Public Health*, 16(14), Article 14. <https://doi.org/10.3390/ijerph16142523>

2. UFP measurements

For the duration of each sampling period, both the FMPS and CPC were co-located in the mobile laboratory. The FMPS integrated particle number consistently reported lower concentrations than the CPC number counts, though the two instruments were highly correlated. SI Figure 2 shows simultaneous FMPS and CPC number counts at each time resolution for data collected in an urban background location.

While sampling restaurant plumes, the concentrations often exceeded the upper detection concentration limit for the CPC. In these cases, an error flag was reported. Due to the frequency of these error flags, we developed a different method to reflect the concentration within the restaurant plumes. Thus, we used the integrated FMPS number and scaled this using the pre-established FMPS:CPC from Figure S2 to determine a reliable measure of PNC in the emission plumes.

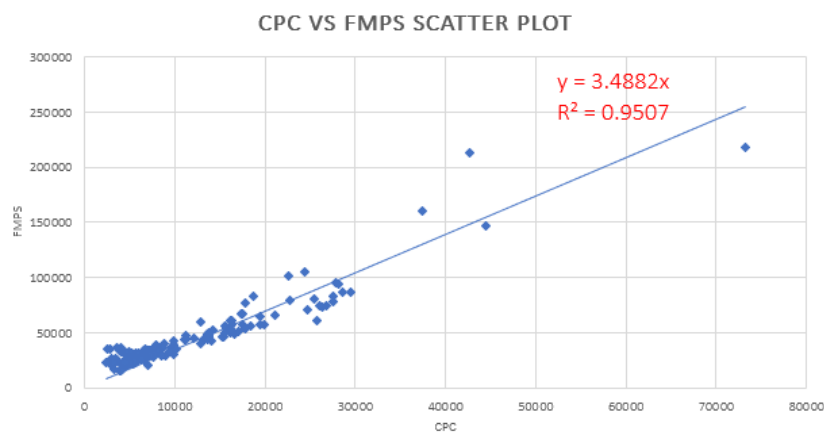


Figure S2. Scatter plot of CPC vs FMPS from the summer field campaign 2019.

Table S1. 5th percentile background ($\mu\text{g}/\text{m}^3$) of OA and BC during the field campaign in this study the fifth percentile of each daily set of data was calculated and defined as the background concentration of OA and BC.

	Background OA, 5th percentile ($\mu\text{g}/\text{m}^3$)	Background BC, 5th percentile ($\mu\text{g}/\text{m}^3$)
Island Cuisine	3.41	0.374
Pizza	3.95	0.428
BBQ	0.42	0.416
Café	3.35	0.820
Beef	2.41	0.352
Diner 1	3.41	0.374
Diner 2	3.95	0.428
Bakery 1	4.12	0.953
Bakery 2	3.06	0.757
Fast Food 1	0.42	0.416
Fast Food 2	3.06	0.757
Bar/Restaurant 1	5.88	1.31
Bar/Restaurant 2	3.35	0.820

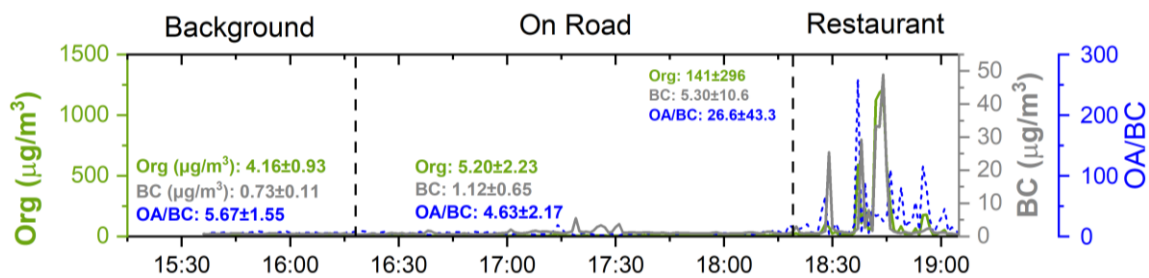
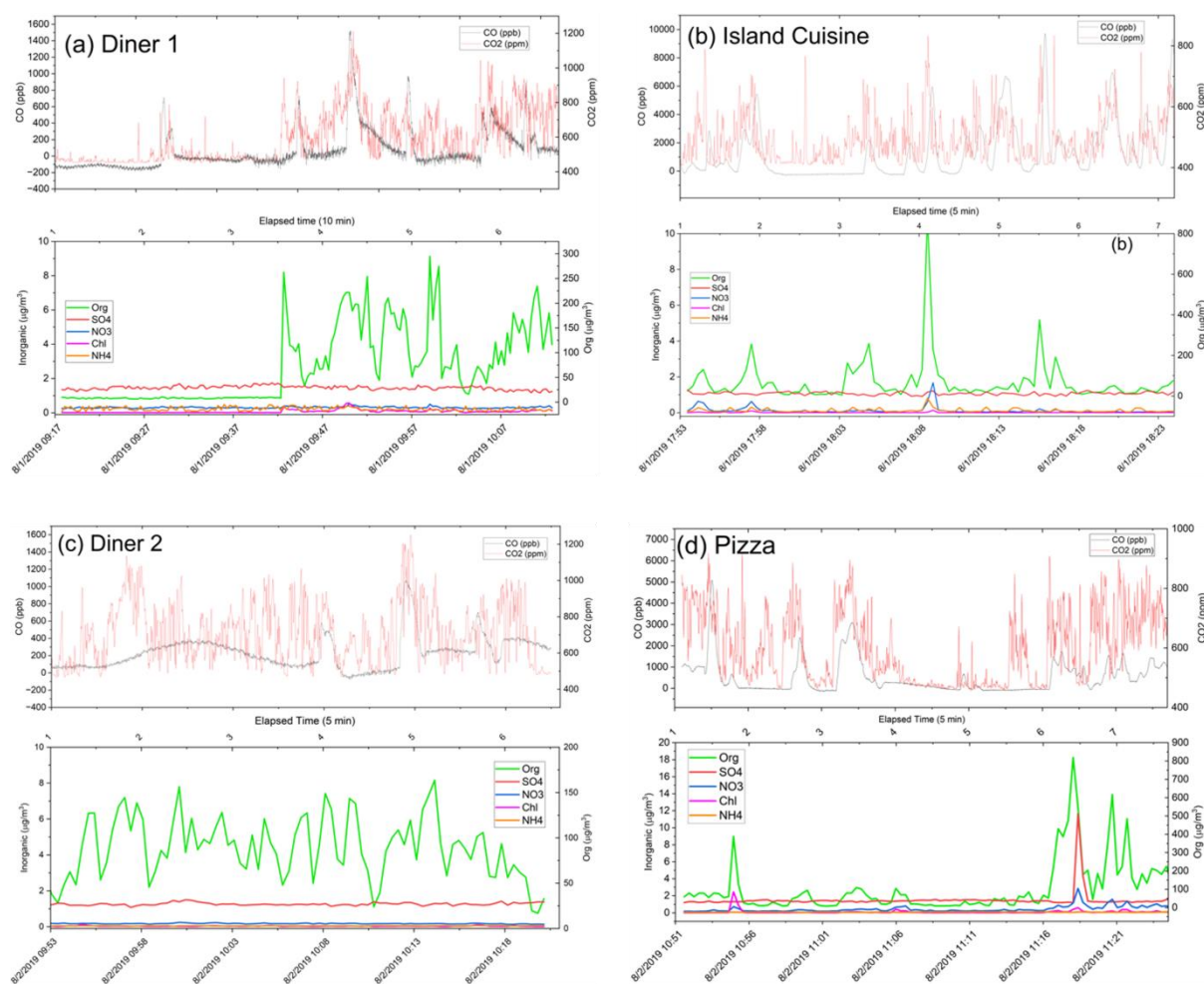
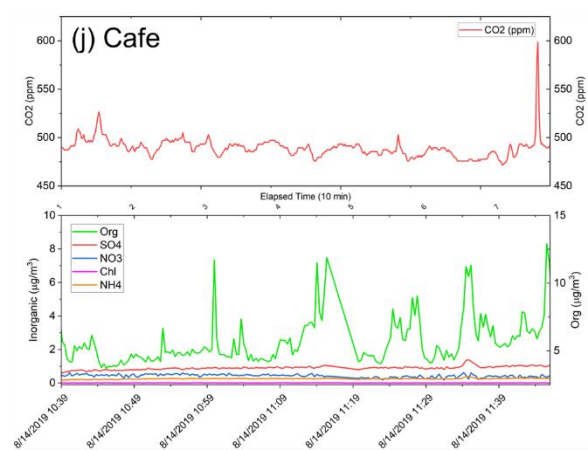
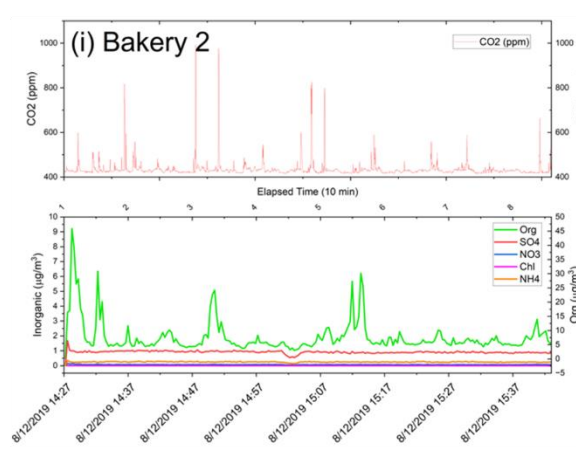
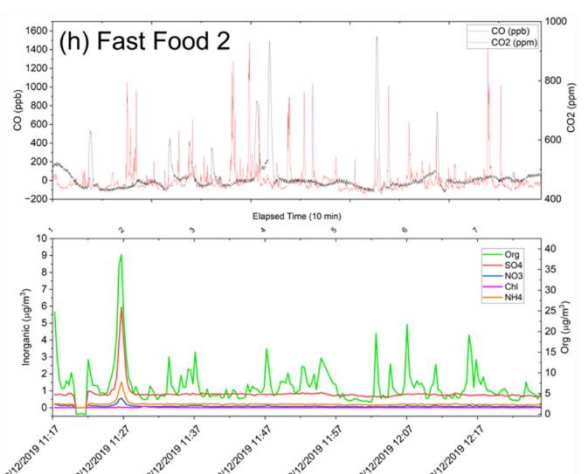
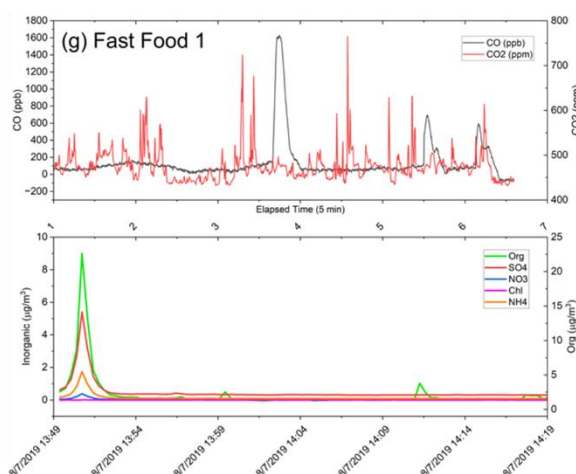
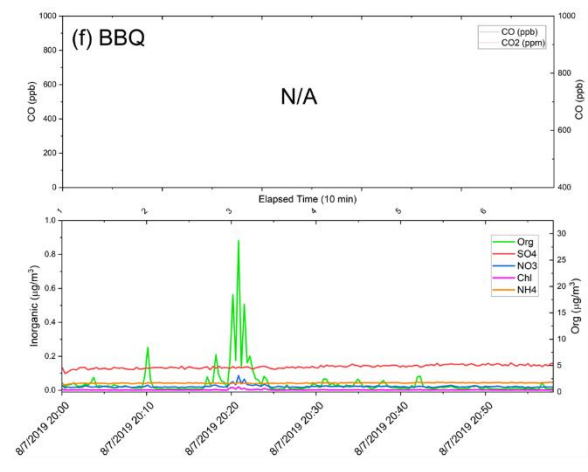
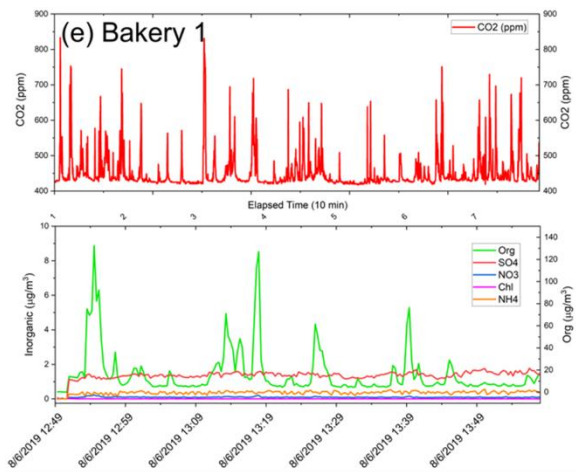


Figure S3. OA/BC time series for the day of the Bar/Restaurant 2 sampling (background, on-road, and restaurant sampling period). The mean OA/BC ratios in the urban background and on-road sampling periods were 5-6. In contrast, the mean OA/BC ratio was significantly higher in the restaurant plume.





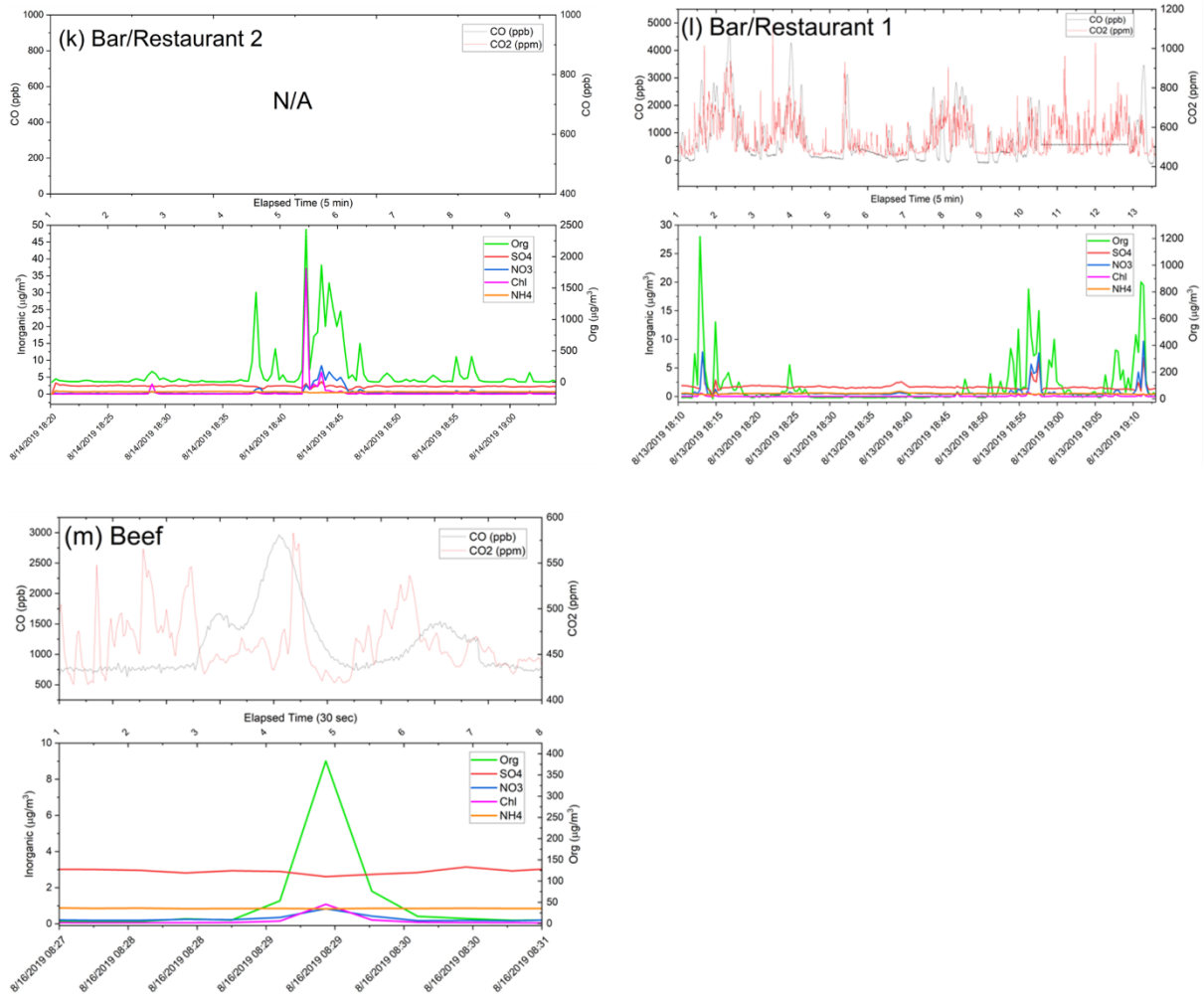
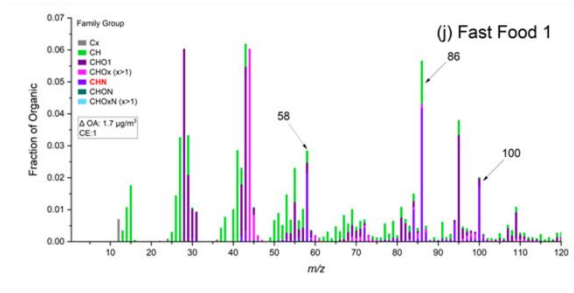
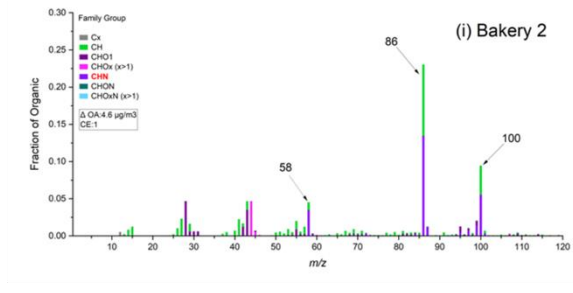
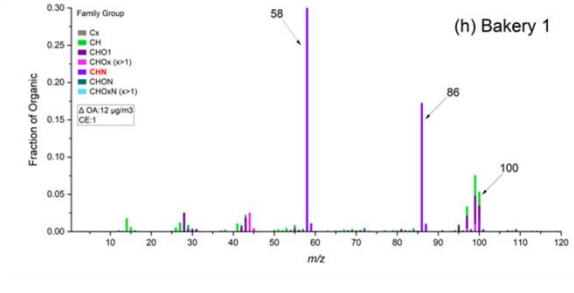
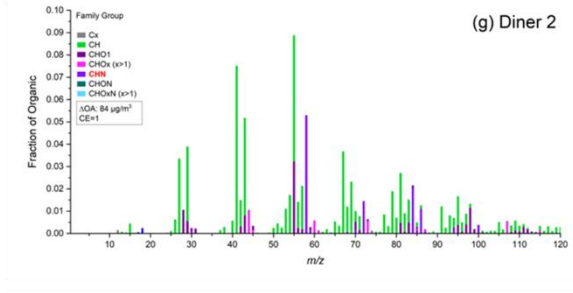
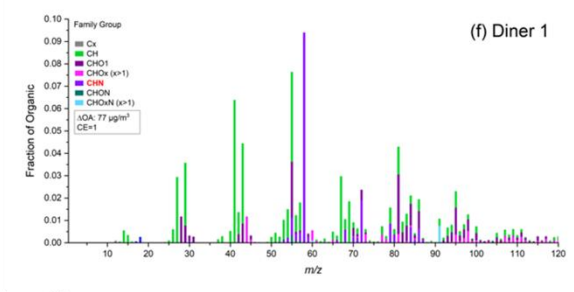
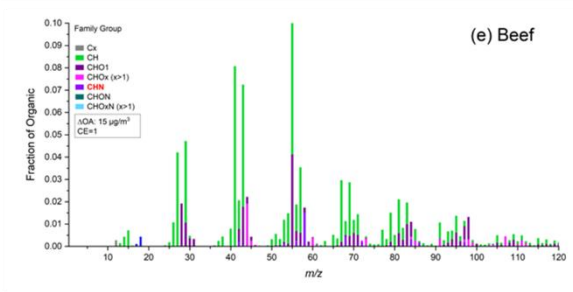
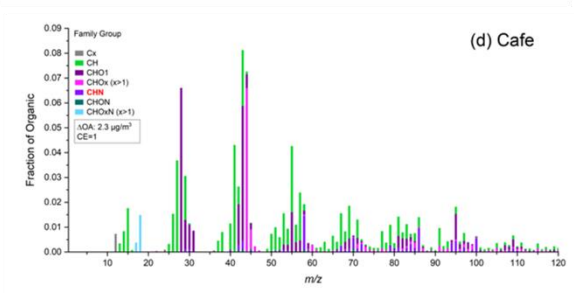
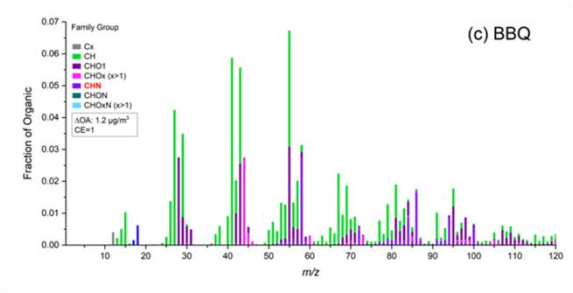
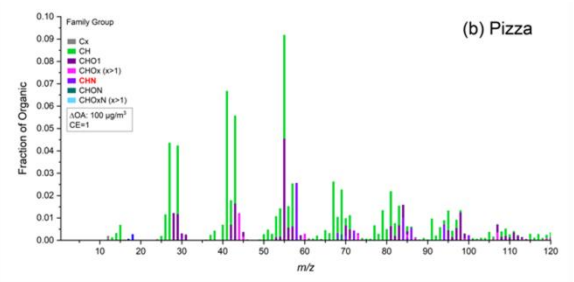
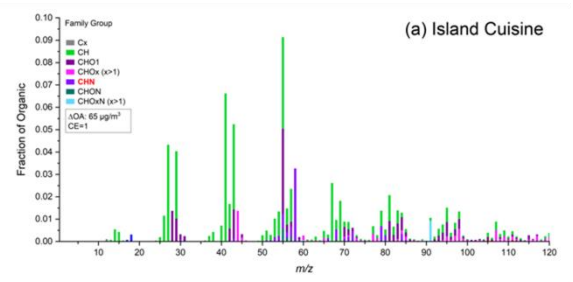


Figure S4. High-resolution time series of organics, sulfate, ammonium, chloride, and nitrate acquired by HR-ToF-AMS is complemented by concurrent CO and CO₂ measurements during restaurant plume observations. Profiles are presented for (a) Diner 1, (b) Island Cuisine, (c) Diner 2, (d) Pizza, (e) Bakery 1, (f) BBQ, (g) Fast Food 1, (h) Fast Food 2, (i) Bakery 2, (j) Café, (k) Bar/Restaurant 2, (l) Bar/Restaurant 1, and (m) Beef. Please note that gas data is absent for (f) BBQ and (k) Bar/Restaurant 2. Only CO₂ measurements are available for (e) Bakery 1, (i) Bakery 2, and (j) Café, with CO data missing.



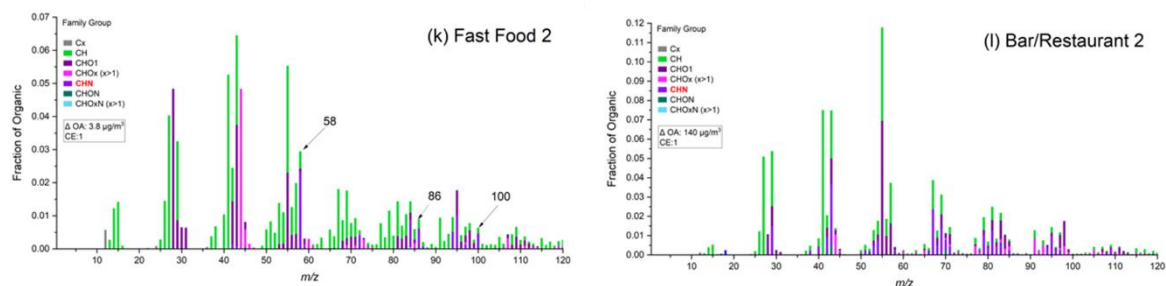


Figure S5. Average AMS cooking mass spectra from other restaurant sites in this study. (a) Island Cuisine, (b) Pizza, (c) BBQ, (d) Café, (e) Beef, (f) Diner 1, (g) Diner 2, (h) Bakery 1, (i) Bakery 2, (j) Fast Food 1, (k) Fast Food 2, and (l) Bar/Restaurant 2.

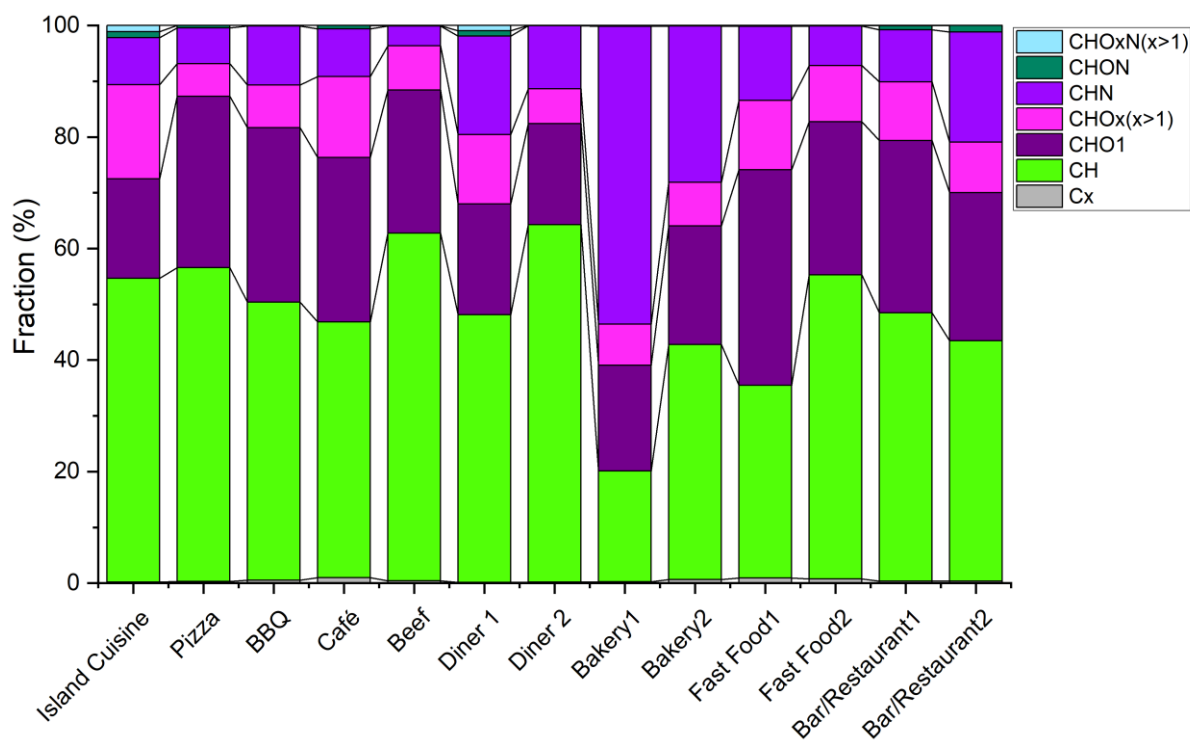
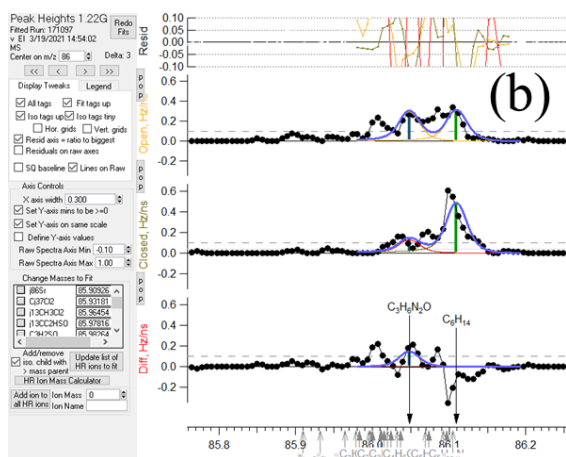
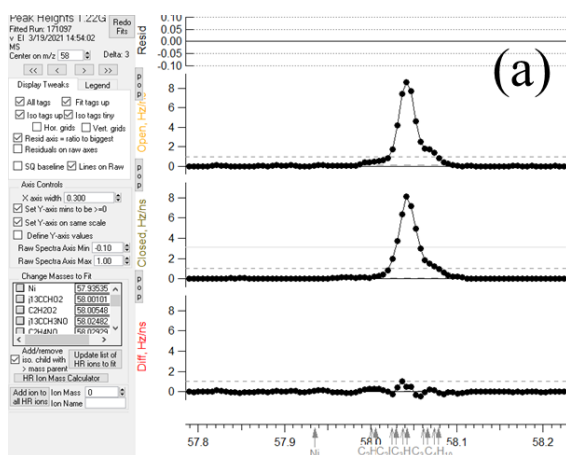


Figure S6. Fractions of CHO_xN , CHON , CHN , CHO_x , CHO1 , CH , and C_x families across cooking sites. Within the distribution of the CHN family group, Bakery 1 and Bakery 2 were observed to have predominant proportions of CHN .

Table S2. Fractions of ions by family group (%) and from three significant nitrogen-containing fragments (%) at m/z 58 ($C_3H_8N^+$), 86 ($C_5H_{12}N^+$), and 100 ($C_6H_{14}N^+$). These reduced nitrogen peaks are the largest in the bakery mass spectra but are not present in the emissions from the majority of the restaurants.

	Cx	CH	CHO1	CHOx(x>1)	CHN	CHON	CHOxN(x>1)	$f_{C_3H_8N^+}$	$f_{C_5H_{12}N^+}$	$f_{C_6H_{14}N^+}$
Island Cuisine	0.196	54.5	17.9	16.88	8.41	1.10	1.11	3.27	0.00	0.00
Pizza	0.284	56.3	30.7	5.88	6.41	0.417	0.009	2.57	0.57	0.23
BBQ	0.538	49.9	31.3	7.65	10.6	0.114	0	2.78	1.66	0.55
Café	0.952	45.9	29.5	14.5	8.60	0.579	0	1.36	0.96	0.55
Beef	0.406	62.3	25.7	7.93	3.56	0.077	0.026	1.51	0.18	0.00
Diner 1	0.138	48.0	19.9	12.5	17.6	0.958	0.958	9.40	0.64	0.00
Diner 2	0.205	64.1	18.1	6.26	11.3	0.020	0	5.30	1.11	0.38
Bakery1	0.265	19.8	19.0	7.37	53.4	0.067	0.082	31.4	17.3	1.63
Bakery2	0.653	42.2	21.3	7.80	28.0	0.049	0.048	3.42	13.5	5.55
Fast Food1	0.889	34.6	38.7	12.4	13.3	0.152	0	2.15	4.18	1.72
Fast Food2	0.742	54.5	27.5	10.1	7.06	0.066	0.047	2.33	0.62	0.47
Bar/Restaurant1	0.365	48.1	31.0	10.5	9.33	0.717	0.043	0.35	0.30	0.11
Bar/Restaurant2	0.342	43.1	26.6	9.02	19.7	1.19	0	0.14	0.05	0.01



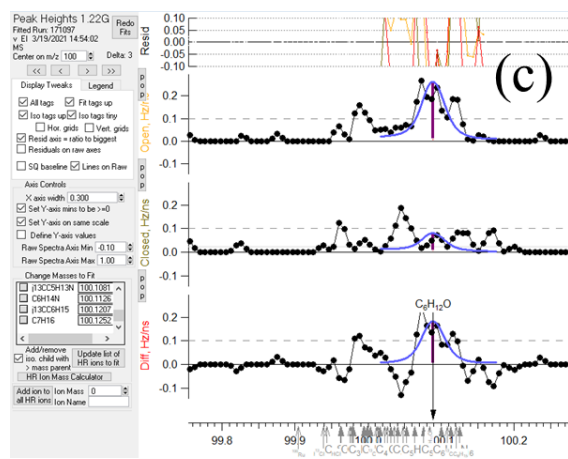


Figure S7. Peak fittings of (a) m/z 58, (b) m/z 86, and (c) m/z 100 from bread baking experiments using Azodicarbonamide ($C_2H_4N_4O_2$, ADA).

3. Validation of Nitrogen-Containing Peak

We addressed the potential issue of refractory components forming on the vaporizer surface, which could influence vaporizer interactions, as highlighted by Allan et al. (2003). Ions from surface ionization, generated at a different location than those from electron ionization, follow a distinct trajectory into the mass spectrometer, resulting in efficiency variances and shifted peaks in mass spectra (Drewnick et al., 2015). Additionally, distinctly irregular or expanded signals from metal ions (e.g., Na^+ and K^+) would imply their origin from the vaporizer surface, suggesting a divergent route for extraction into the MS.

To ascertain the presence of nitrogen-containing peaks in our mass spectrum and these fragments are not from surface ionization, we have confirmed that ions such as Na^+ and K^+ displayed peak configurations akin to Ar^+ , as illustrated in Figure S9. The consistency in peak shape and width shows that these ions are not from irregular signals. Subsequently, Figure S8 showcased the peak alignment of nitrogen-containing fragments, affirming their authentic presence. This was further corroborated by the nonexistence of signals during the chopper's inactivity, eliminating the possibility of internal instrumental discrepancies. Thus, our observation shows that our fragments seemingly do not emanate from the surface of the vaporizer.

References:

- Allan, J. D., Alfarra, M. R., Bower, K. N., Williams, P. I., Gallagher, M. W., Jimenez, J. L., ... & Worsnop, D. R. (2003). Quantitative sampling using an Aerodyne aerosol mass spectrometer 2. Measurements of fine particulate chemical composition in two UK cities. *Journal of Geophysical Research: Atmospheres*, 108(D3).
- Drewnick, F., Diesch, J.-M., Faber, P., & Borrmann, S. (2015). Aerosol mass spectrometry: Particle–vaporizer interactions and their consequences for the measurements. *Atmospheric Measurement Techniques*, 8(9), 3811–3830. <https://doi.org/10.5194/amt-8-3811-2015>

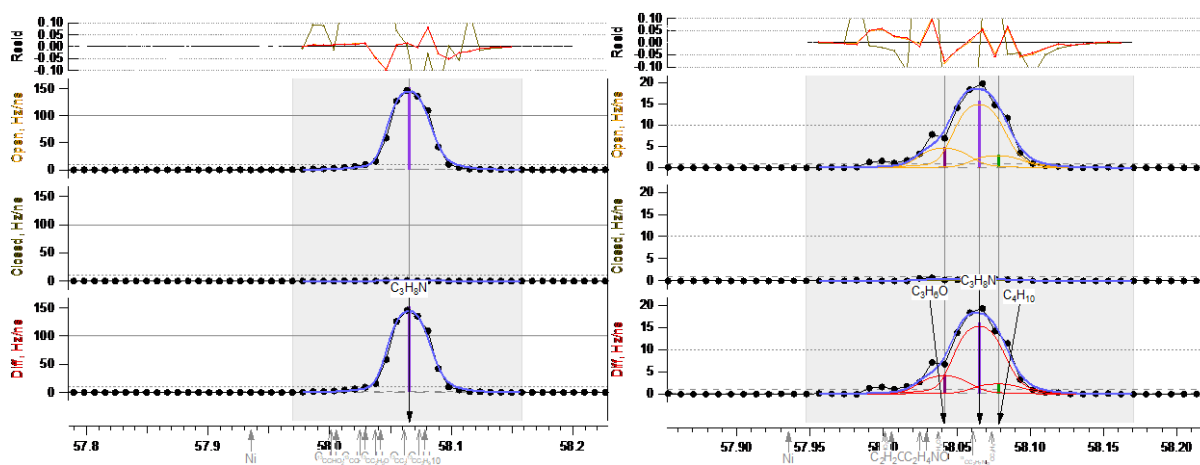


Figure S8. Example Peak Fitting at m/z 58 for Bakery 1 (left) and Bakery 2 (right): This demonstrates the minimal signal observed when the chopper was in the closed position.

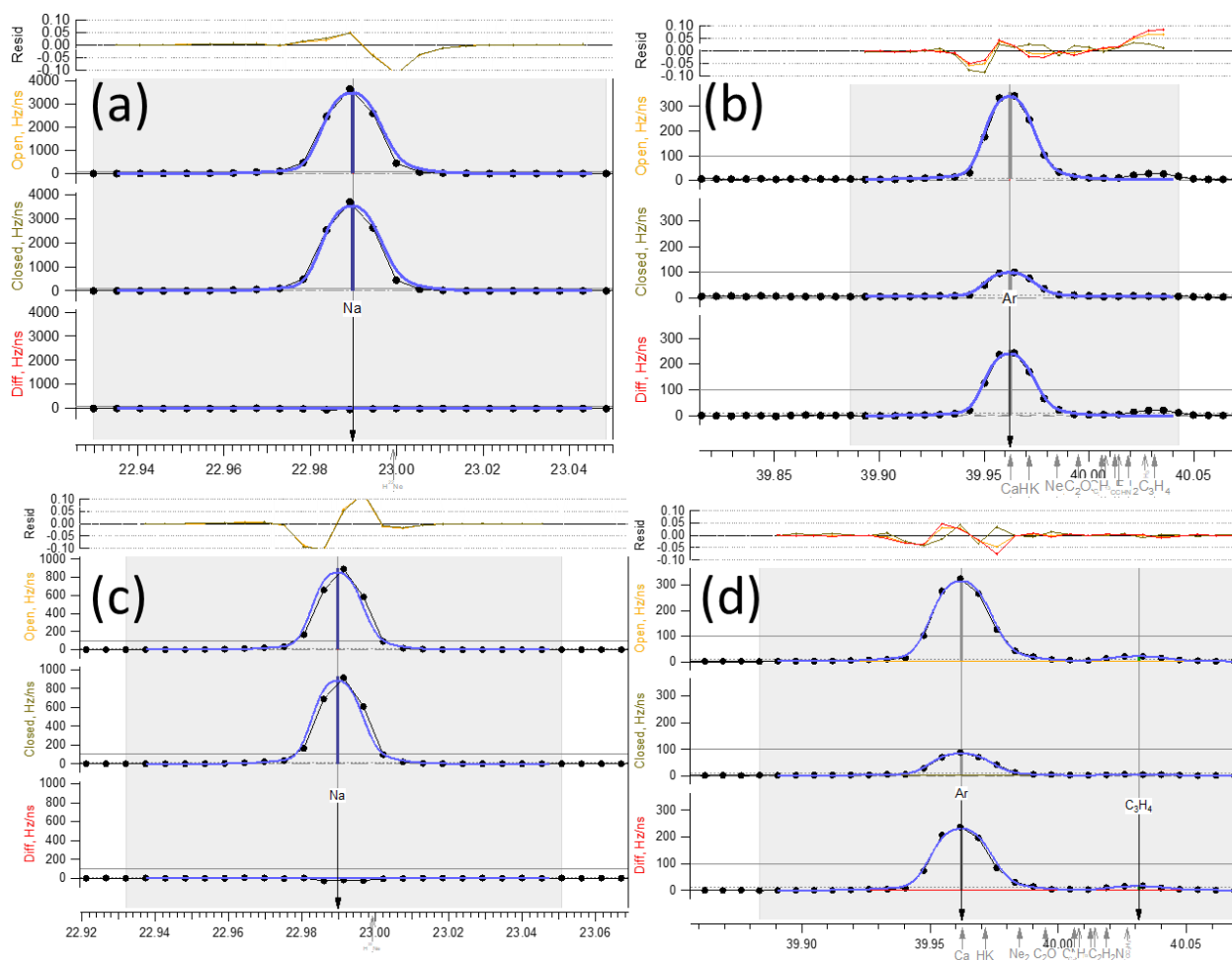


Figure S9. Comparative Analysis of Ion Peak Shapes from Bakery 1 and Bakery 2. The figure presents a side-by-side comparison of peak shapes and widths for Na^+ (left) and Ar^+ (right) from Bakery 1 (a & b) and Bakery 2 (c & d). Na^+ and K^+ signals, as exemplified by the Na^+ signal in this figure, are neither irregular nor distinctively different from the Ar^+ peak. All peaks, from (a) to (d), display a consistent 2σ width of approximately 0.04 m/z, supporting the hypothesis that these ions aren't products of surface ionization.

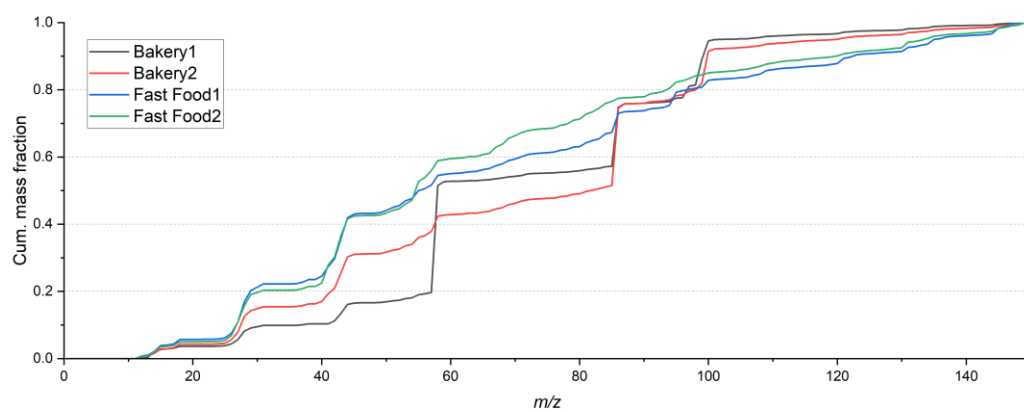


Figure S10. Comparative Cumulative Mass Fraction Diagram: This illustrates the contribution of m/z signals at different culinary locations (Bakery 1 & 2, Fast Food 1 & 2). The plot serves to highlight the varying contributions to the mass spectra from each site.

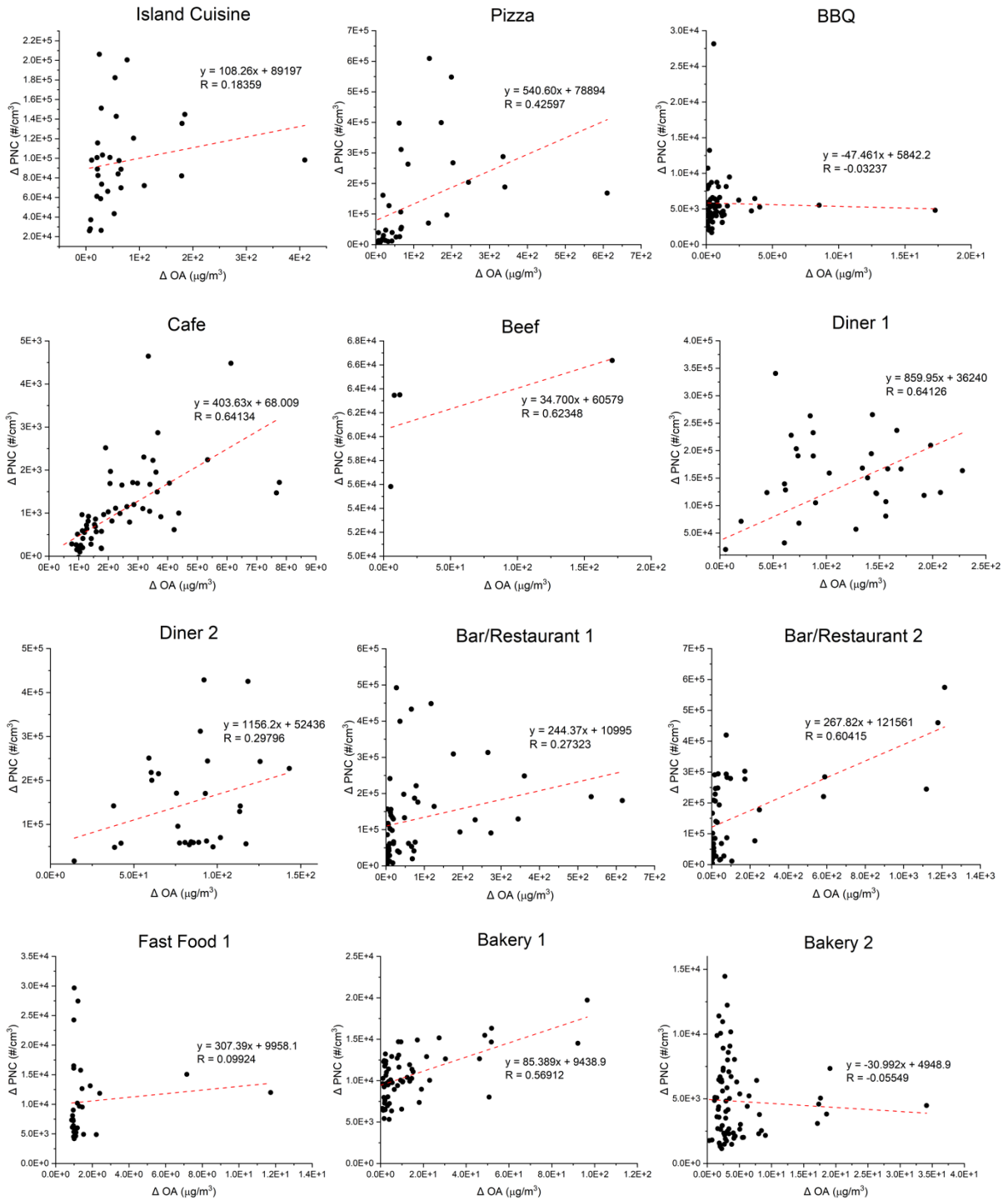


Figure S11. Scatter plot and correlation coefficient of ΔPNC ($\#/cm^3$) vs ΔOA ($\mu g/m^3$) across 13 cooking sites in this study. There is no strong linear correlation between ΔPNC and ΔOA with R (<0.7).

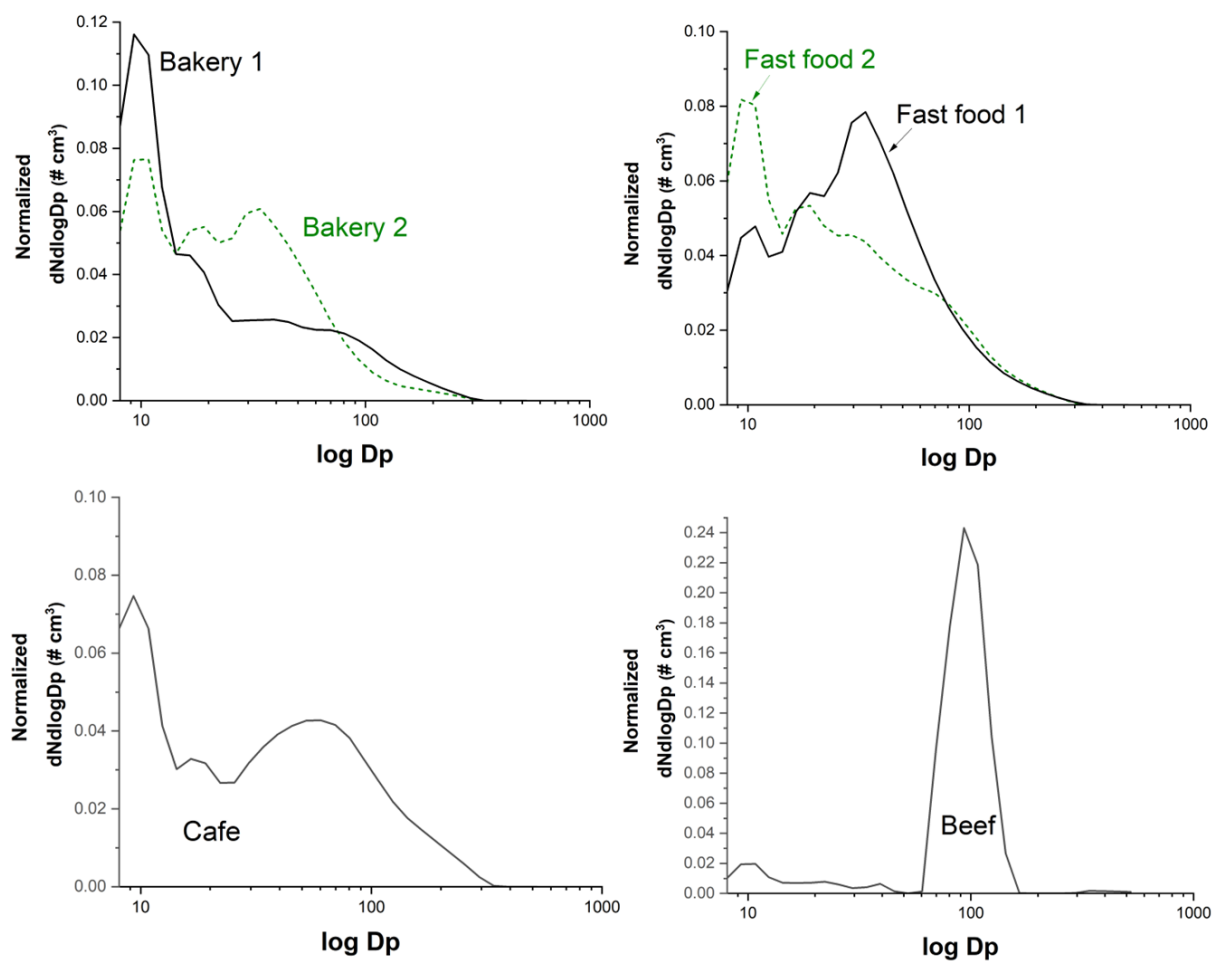


Figure S12. Particle size and total particle number distributions of cooking samples with lower PNC concentrations.

4. LC-MS/MS Offline sample preparation and analysis

After MS compound formulas were generated from high mass resolution (within 2 ppm) data, and underwent QC/QA, including background subtraction and formula composition checks, target lists were created for each sample and used to analyze the compounds of interest with tandem mass spectrometry. As there were less than 200 compounds of interest for each sample, all MS compounds which passed QC/QA were included in the target lists.

SIRIUS 5.6.3 was used to analyze the LC-MS/MS samples, and an updated version of the R code that formats the updated exported SIRIUS results to work with the Python APPI code can be provided for MS/MS analysis if requested. SIRIUS was used with a free academic/non-commercial user account, and more information can be found at <https://bio.informatik.uni-jena.de/software/sirius/> for future updates and information on SIRIUS 5.

Table S3. Offline filter sample volumes and sampling times.

Date	Day of Week	Location	Sample Volume (L)	Sample Start Time (EST)	Sample End Time (EST)
8/1/19	Thursday	Diner 1	2,250	9:42:00	10:12:00
8/1/19	Thursday	Island Cuisine	1,890	17:54:00	18:24:00
8/2/19	Friday	Urban Background 1	2,624	14:16:00	17:00:00
8/2/19	Friday	Diner 2	1,764	9:52:00	10:20:00
8/2/19	Friday	Pizza	2,079	10:52:00	11:25:00
8/5/19	Monday	Field Blank			
8/5/19	Monday	Urban Background 2	2,898	5:39:00	6:25:00
8/6/19	Tuesday	Urban Background 3	5,607	9:48:00	11:17:00
8/6/19	Tuesday	Bakery 1	4,095	12:49:00	13:54:00
8/7/19	Wednesday	Fast Food 1	2,520	1:34:00	2:14:00
8/9/19	Friday	Urban Background 4	4,860	13:37:00	14:58:00
8/9/19	Friday	Linwood Asphalt	3,840	10:00:00	11:04:00
8/12/19	Monday	Fast Food 2	3,840	11:22:00	12:26:00
8/12/19	Monday	Bakery 2	4,560	14:27:00	15:43:00
8/13/19	Tuesday	Bar/Restaurant 1	3,304	18:14:00	19:10:00
8/13/19	Tuesday	Field Blank			
8/14/19	Wednesday	Cafe	3,953	10:39:00	11:46:00
8/14/19	Wednesday	Urban Background 5	4,307	15:36:00	16:49:00
8/14/19	Wednesday	Bar/Restaurant 1	2,596	18:20:00	19:04:00

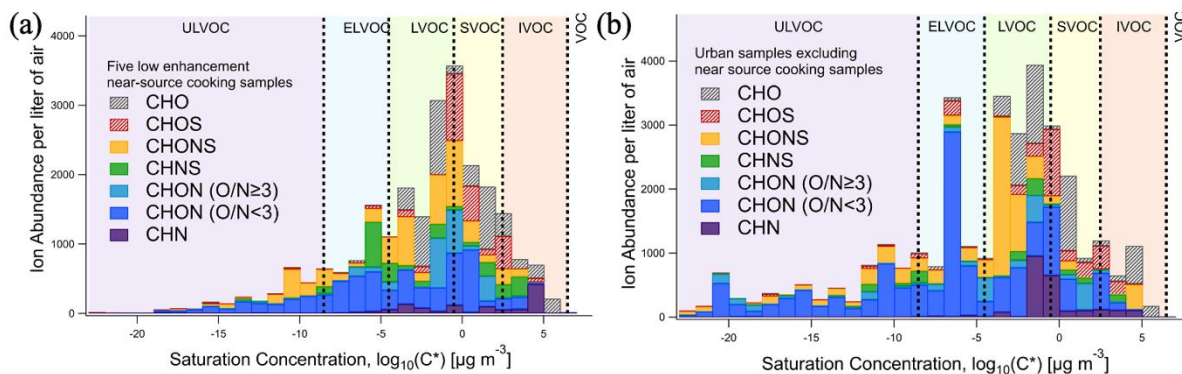


Figure S13. Averaged chemical composition of particle-phase functionalized organic compounds from (a) five lower enhanced near-source cooking samples (bakery 1, bakery 2, fast food 1, fast food 2, café), (b) other urban samples excluding near-source cooking samples. In Table S3, the five urban background samples are all included in (b). Supplementary figures are provided to accompany Figure 7.

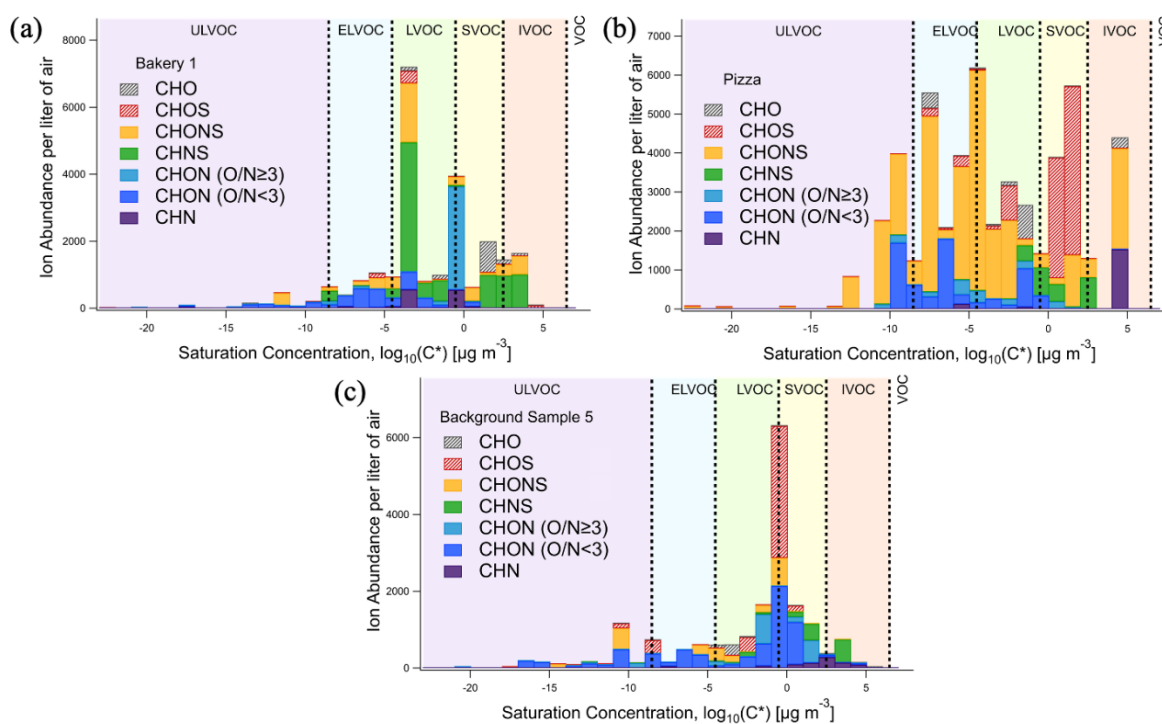


Figure S14. LC-TOF speciation of Bakery 1, Pizza, and Urban Background 5 samples, shown as compound class volatility distributions. Supplemental figures are provided as they are the samples selected for MS/MS analysis.

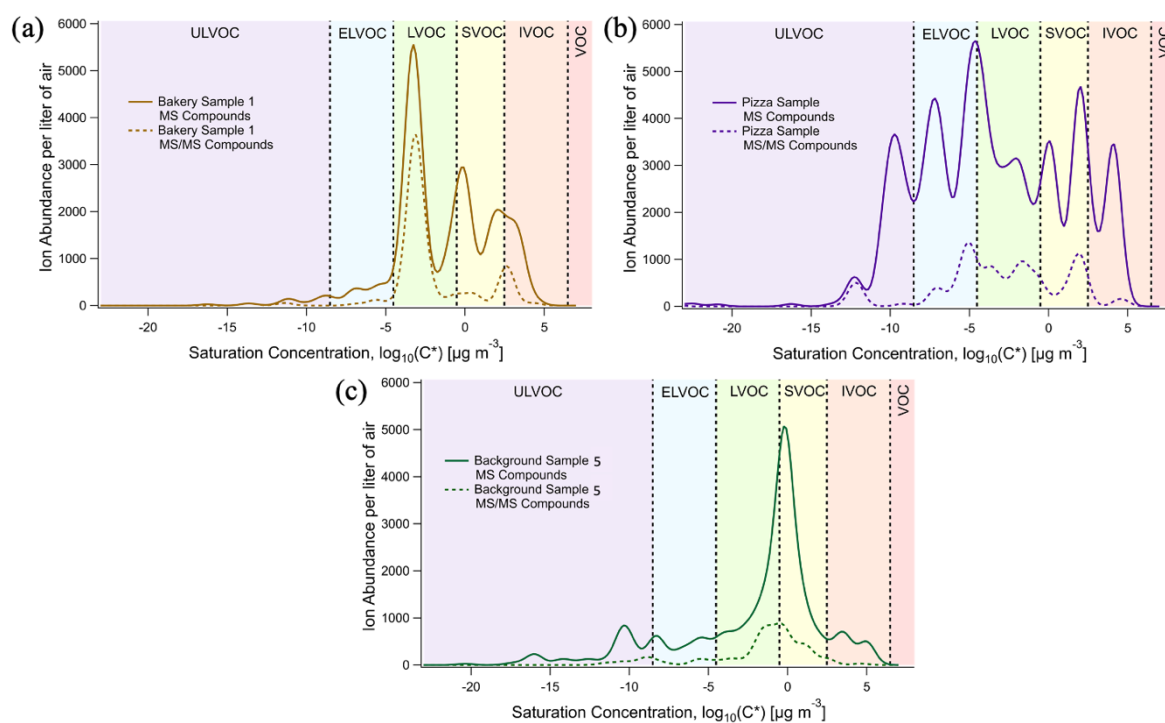


Figure S15. Ion abundance volatility distributions of compounds characterized with LC-MS/MS compared to LC-TOF compounds, for (a) Bakery sample 1, (b) Pizza sample, and (c) urban background sample 5. Notes: For the three samples selected for MS/MS analysis, on average, 24.8% of targeted compounds were observed via MS/MS and assigned functionalities, with an average of 21.4% of the total MS abundance observed via MS/MS. This figure shows the compound class volatility distribution of MS/MS observed compounds for each sample compared to the abundance from all MS compounds. While not all compounds were observed, the MS/MS compounds were from a range of volatilities and compound classes. The volatility distributions of the particle-phase organic compounds' chemical composition at each of these three sites can be found in Figure S11.

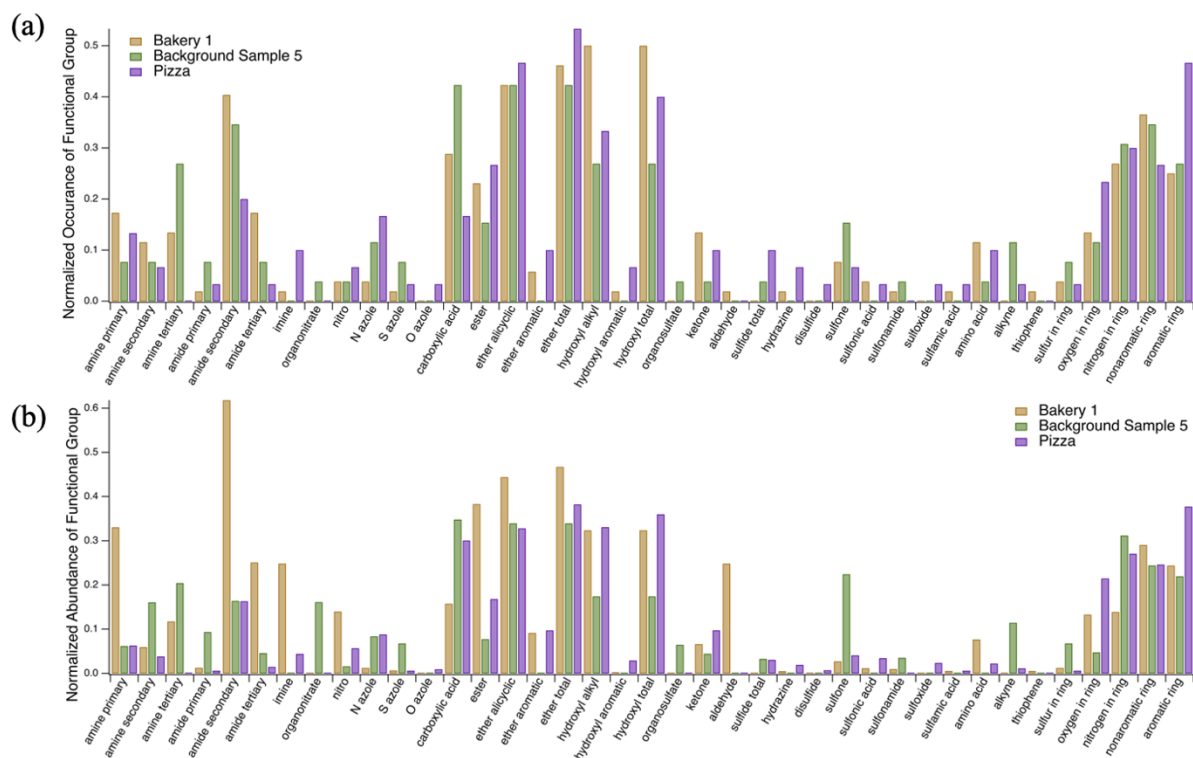


Figure S16. The functional groups and structural features observed in Bakery 1 (gold), Pizza (purple), and urban background sample 5 (green) by the (a) number of occurrences and (b) relative abundance of each functional group or structural features. The structural features are on the far right (i.e., ringed species), and the nitrogen-containing functional groups are on the left. The distributions represent the relative occurrence or abundance of a functional group within that sample's MS/MS analyzed compounds. Similar to prior work, the occurrence of organonitrates is lower than expected due to potential losses and poor ionization of organonitrates (Ditto et al., 2020); however, there are additional CHON functional groups observed, such as nitro, and some oxygen-containing azoles (grouped into azoles in Figure 8).

Other functional groups searched for but not seen in these samples are listed below.

1. peroxide
2. hydroperoxide
3. carbonylperoxynitrate
4. carbonylperoxyacid
5. peroxy nitrate
6. nitroester
7. nitrophenol
8. nitrile
9. anhydride
10. isocyanate
11. isothiocyanate
12. oxime
13. enamine
14. azide
15. hydrazone
16. nitroso

17. carbothioester
18. thiol
19. thioamide
20. sulfinat
21. sulfinic_acid
22. sulfonate
23. carboazosulfone
24. alt_sulfoxide
25. sulfuric acid diester
26. sulfamate
27. sulfenic acid
28. sulfenate
29. thioketone
30. thial
31. diazene
32. azoxy nitrogen
33. diazo nitrogen
34. azo
35. isonitrile
36. carbothiocarboxylate